SCALING PROPERTIES OF WILSON LOOPS PIERCED BY P-VORTICES

A thesis presented to the faculty of
San Francisco State University
In partial fulfilment of
The Requirements for
The Degree

Master of Science
In
Physics

by

Patrick Apollo Dunn

San Francisco, California

May 2018

CERTIFICATION OF APPROVAL

I certify that I have read *SCALING PROPERTIES OF WILSON LOOPS PIERCED BY P-VORTICES* by Patrick Apollo Dunn and that in my opinion this work meets the criteria for approving a thesis submitted in partial fulfillment of the requirements for the degree: Master of Science in Physics at San Francisco State University.

Jeff Greensite
Professor of Physics

Susan Lea
Professor of Physics

Kristan Jensen
Assistant Professor of Physics

SCALING PROPERTIES OF WILSON LOOPS PIERCED BY P-VORTICES

Patrick Apollo Dunn
San Francisco State University
2018

A center vortex is a special type of fluctuation in the Yang-Mills vacuum that appears to be responsible for the phenomenon known in physics as quark confinement. The main point of my research was to test if excitations on the center-projected Z_N lattice known as P-vortices are effective at locating center vortices, and therefore correlated with gauge-invariant observables. This was done by studying the ratios of expectation values for Wilson loops associated with one P-vortex piercing, to those of Wilson loops associated with zero P-vortex piercings. The classification of the Wilson loops was done on the Z_2 lattice, but the calculations of the Wilson loop expectation values were done on the unprojected $SU(2)$ lattice. We then plotted these ratios versus loop area in physical units, for a range of lattice couplings. The data points fall approximately on a single curve, consistent with scaling. Surprisingly, the ratios are rather insensitive to the location of the vortex piercing within the Wilson loop.

I certify that the Abstract is a correct representation of the content of this thesis.

Jeff Greensite 5-18-2018

Chair, Thesis Committee Date

ACKNOWLEDGMENTS

I would like to thank my parents, Vera and Lawrence Dunn, for always supporting me in my academic endeavors. I would also like to thank my advisor, Dr. Jeff Greensite, for showing incredible patience with me.

TABLE OF CONTENTS

LIST OF FIGURES

Chapter 1

Introduction to the Quark Confinement Problem

1.1 Quarks

The phenomenon in physics known as quark confinement has yet to be completely explained and research in this field promises a greater understanding of nature at a fundamental level. Quarks are the elementary particles that interact through the strong nuclear force; they do also interact via the other three forces (electromagnetic, nuclear weak, and gravity), but only the strong nuclear force is important for quark confinement. Confinement refers to the fact that quarks have only been observed in bound groups of two (quarks and anti-quark pairs known as mesons) or three (baryons) in special so-called color neutral configurations. Protons and neutrons are well-known examples of baryons (electrons belong to another class called leptons).

Quarks are confined in the sense that a quark has never been observed to be moving about free of the immediate influence of another quark.

1.2 String Tension

If the potential between two quarks is proportional to the distance between them, then the two quarks can never be separated. The relation between the potential and distance is $V(r) \sim \sigma r$, where σ is the string tension. If the quarks are pulled apart, the restoring energy of the linear potential grows sufficiently rapidly to prevent them from being separated. The potential energy takes the form of a color electric flux tube between the two quarks. This flux tube is often referred to as a string, and the energy per unit length of the flux tube is known as the string tension. The accepted value of the string tension is approximately $(440\ \text{MeV})^2$. This value is obtained experimentally from the inverse slope of graphs, known as Regge trajectories, of Spin vs $(\text{Mass})^2$ for mesons and baryons. The string between the quarks may break, creating a new quark-antiquark pair. In a non-confining theory the potential may go asymptotically to a constant, but there is no string breaking and you can have isolated color charges.

At very short distances, much less than a Fermi, the strength of quark interaction is extremely weak in terms of the effective (or running) constant. Therefore quarks bound within protons and neutrons, as well as those bound within other baryons and mesons, feel a relatively weak nuclear strong force. This phenomenon is known

as asymptotic freedom, referring to the fact that quarks effectively become free of each other's influence as the distance between them decreases; the effective coupling constant of the interaction becomes asymptotically weaker.

A full theory of the nuclear strong force therefore needs to contain both of these features of quark interaction, a linearly increasing potential at large distances and an asymptotically decreasing coupling constant at very short distances.

Chapter 2

Quantum Field Theory and Gauge Invariance

2.1 Path Integral Formulation of Quantum Field Theory

Quantum field theory provides the framework under which quark interactions may be calculated. The most promising theory for quark interactions was developed from the path integral formulation of quantum field theory. In this formulation the amplitude for a transition from an initial state to a final state is given as a sum over the amplitude of all possible paths between the two states.

$$U(\phi_{final}, \phi_{initial}; dt) = \sum_{all\,paths} e^{i\cdot(phase)} \tag{2.1}$$

The amplitude, $e^{i\cdot(phase)}$, for each path is proportional to $e^{(iS/\hbar)}$, where S is the relativistic action given by

$$S = \int L(\phi, \partial_\mu \phi) d^4x \tag{2.2}$$

The sum over all paths becomes a functional integral

$$U(\phi_{final}, \phi_{initial}; dt) = \int_{-\infty}^{+\infty} D\phi e^{i\int d^4x L} \tag{2.3}$$

The Lagrangian can be separated into free-field terms, interaction terms, and source terms. Scattering cross sections and decay rates are obtained from the path integral by expanding the exponential as a Taylor series in terms of the interaction and source parameters of the Lagrangian. This corresponds to a small perturbation of the Lagrangian via an interaction parameter. Feynman diagrams pictorially represent these series terms and are a popular tool for calculations in quantum field theory.

2.2 Gauge Invariance

The Lagrangian is therefore key to the path integral formulation of quantum field theory. The principle of gauge invariant Lagrangians led to the development of the Standard Model of strong, electromagnetic, and weak interactions. I will first show three examples of gauge invariance from classical electrodynamics, relativistic electrodynamics, and quantum non-relativistic electrodynamics in order to motivate

the full theory of gauge invariance within the framework of quantum field theory.

2.2.1 Examples of Gauge Invariance

Classical Electrodynamics

The physical electric and magnetic fields can be formulated in terms of electric and magnetic potentials. I will utilize throughout the particle physics convention of setting $c = \hbar = 1$. Using Heaviside-Lorentz units, these equations take the form

$$\mathbf{B} = \nabla \times \mathbf{A} \tag{2.4}$$

$$\mathbf{E} = -\nabla V - \partial \mathbf{A}/\partial t \tag{2.5}$$

These potentials allow electrodynamics to be simplified from Maxwell's four equations to only two. Although classically only the electric and magnetic fields can be measured, quantum mechanically the potentials can be observed in the Aharonov-Bohm effect. The values for $\mathbf{E}$ and $\mathbf{B}$ are unaffected by the following transformations of the potentials involving the scalar function λ :

$$\mathbf{A} \rightarrow \mathbf{A} + \nabla\lambda \tag{2.6}$$

$$V \rightarrow V - \partial\lambda/\partial t \tag{2.7}$$

In other words, the classical electromagnetic equations are invariant under such a gauge transformation.

Relativistic Electrodynamics

Since the object is to consider relativistic quantum field theory, it is useful to introduce relativistic notation, in which the electromagnetic potentials are written in terms of a four-vector

$$A^{\mu} = (V, \mathbf{A}) \tag{2.8}$$

and Maxwell's equations then take the following form in terms of the four-vector.

$$\partial^{\mu}\partial_{\nu}A^{\nu} - \partial^{\nu}\partial_{\nu}A^{\mu} = \mu_0 J^{\mu} \tag{2.9}$$

where J^{μ} is the external charge/current 4-vector. This set of equations is unaffected by the following transformation of the potential fields involving the scalar function λ:

$$A^{\mu} \rightarrow A^{\mu} + \partial^{\mu}\lambda \tag{2.10}$$

So the relativistic formulation of classical electrodynamics is also invariant under the specified gauge transformation.

Non-relativistic Quantum Mechanics

Another example of gauge invariance arises in non-relativistic quantum mechanics. If we assume that ψ satisfies the Schrödinger equation for an electromagnetic Hamiltonian,

$$i\frac{\partial\psi}{\partial t} = \left[\frac{1}{2m}(-i\nabla - q\mathbf{A})^2 + qV\right]\psi \tag{2.11}$$

and we apply the previous gauge transformations to the electromagnetic fields

$$\mathbf{A} \rightarrow \mathbf{A} + \nabla\lambda \tag{2.12}$$

$$V \rightarrow V - \partial\lambda/\partial t \tag{2.13}$$

then we must apply the transformation

$$\psi \rightarrow \psi' = e^{iq\lambda}\psi \tag{2.14}$$

in order to satisfy the Schrödinger equation with the transformed fields.

2.2.2 Invariance of Dirac Lagrangian - QED

Now let's move forward to a gauge invariant theory for electrodynamics within the framework of quantum field theory. Let's examine the effect of a global phase change

on the Dirac Lagrangian for spin 1/2 particles:

$$\mathcal{L}_{DIRAC} = i\bar{\psi}\gamma^{\mu}\partial_{\mu}\psi - m\bar{\psi}\psi \tag{2.15}$$

If we apply the global phase transformation $\psi \rightarrow e^{iq\theta}\psi$, where θ is any real number, then $\bar{\psi} \rightarrow \bar{\psi}e^{-iq\theta}$. The q represents the charge magnitude of an electron. The two phase changes cancel each other in each term, thereby leaving the Lagrangian unchanged.

If we now apply a local phase transformation, $\psi \rightarrow e^{iq\theta(x^{\mu})}\psi$, where θ is a function of spacetime x^{μ}, then the derivative acts on θ as well

$$\partial_{\mu}(e^{iq\theta}\psi) = e^{iq\theta}\partial_{\mu}\psi + iqe^{iq\theta}\psi\partial_{\mu}\theta \tag{2.16}$$

and so an extra term now appears in the Lagrangian.

$$\begin{aligned} \mathcal{L}' &= i\bar{\psi}\gamma^{\mu}\partial_{\mu}\psi - m\bar{\psi}\psi - q\bar{\psi}\gamma^{\mu}\psi\partial_{\mu}\theta \\ &= \mathcal{L}_{DIRAC} - q\bar{\psi}\gamma^{\mu}\psi\partial_{\mu}\theta \end{aligned} \tag{2.17}$$

The Lagrangian needs to be modified in order to satisfy local gauge invariance. This can be accomplished by adding a vector gauge field A_{μ} and requiring that it transforms as

$$A_{\mu} \rightarrow A_{\mu} - \frac{1}{q}\partial_{\mu}\theta, \tag{2.18}$$

and replacing the original derivative with the operator known as the covariant derivative

$$D_\mu = \partial_\mu + iqA_\mu. \tag{2.19}$$

The Lagrangian now reads as

$$\mathcal{L} = i\bar{\psi}\gamma^\mu D_\mu \psi - m\bar{\psi}\psi \tag{2.20}$$

The covariant derivative results in an additional term that cancels out the extra term, and so the modified Lagrangian satisfies local gauge invariance. This new term in the Lagrangian corresponds to an interaction between the Dirac field ψ and the gauge field A_μ. The gauge field needs its own free field terms in the Lagrangian. The Lagrangian for a free field of spin 1 is represented by the electromagnetic gauge field

$$\mathcal{L} = \frac{1}{16\pi} F^{\mu\nu} F_{\mu\nu} \tag{2.21}$$

$$F^{\mu\nu} = \partial^\mu A^\nu - \partial^\nu A^\mu \tag{2.22}$$

This Lagrangian can also be written classically in terms of the electric and magnetic fields

$$\mathcal{L} = \mathbf{E}^2 - \mathbf{B}^2 \tag{2.23}$$

The final Lagrangian happens to be the QED Lagrangian

$$\mathcal{L}_{QED} = i\bar{\psi}\gamma^{\mu}D_{\mu}\psi - m\bar{\psi}\psi - \frac{1}{16\pi}F^{\mu\nu}F_{\mu\nu} \tag{2.24}$$

which is invariant under the transformations

$$\psi \rightarrow e^{iq\theta(x^{\mu})}\psi \tag{2.25}$$

$$A_{\mu} \rightarrow A_{\mu} - \frac{1}{q}\partial_{\mu}\theta \tag{2.26}$$

To recapitulate, if we require the Lagrangian for a spin 1/2 field, the Dirac field, to be invariant under the gauge transformation, $\psi \rightarrow e^{iq\theta(x^{\mu})}\psi$, then we must replace the derivative with the covariant derivative $D_{\mu} = \partial_{\mu} + iqA_{\mu}$, thereby introducing a gauge field to the Lagrangian that must transform as $A_{\mu} \rightarrow A_{\mu} - \frac{1}{q}\partial_{\mu}\theta$. Lastly, the gauge field requires its own free field term, $F^{\mu\nu}F_{\mu\nu}$, in order to propagate.

2.2.3 Yang-Mills theory

Noting that $e^{i\theta}$ is a one-dimensional unitary matrix U(1), the above procedure is known as U(1) gauge invariance. Yang-Mills theory involves extending the previous method to gauge groups SU(N), the group of all unitary matrices of determinant one, The transformation $e^{i\theta}$ is generalized to $e^{iH(N)}$, H being a traceless Hermitian

N×N matrix. ψ then is composed of N Dirac spinors.

$$\psi_\alpha = \begin{pmatrix} \psi_\alpha^1 \\ \psi_\alpha^2 \\ \vdots \\ \psi_\alpha^N \end{pmatrix} \tag{2.27}$$

The number of color components required correlates to N of SU(N), i.e. the number of "colors" in the theory. The Hermitian matrices used can be written in the form

$$H = a \cdot \tau \tag{2.28}$$

where τ represents the $N^2 - 1$ generator elements of SU(N) and a is an $N^2 - 1$ dimensional vector. In this case, the group elements, $U = e^{iH}$, don't commute, as they do in U(1) gauge theory. Gauge theories with non-commuting matrices are known as non-Abelian gauge theories. In order to maintain gauge invariance, the covariant derivative is slightly modified, and an extra term is now necessary in the transformation of the gauge fields.

$$\psi \to e^{iga\cdot\tau}\psi \tag{2.29}$$

$$D_\mu = \partial_\mu + ig\tau \cdot A_\mu \tag{2.30}$$

$$A^i_\mu \to U(x)A^i_\mu U^\dagger(x) + \frac{i}{g}U(x)\partial_\mu U^\dagger(x) \tag{2.31}$$

where $U = e^{iH}$, $U^\dagger = e^{-iH}$. The infinitesimal transformation is

$$A^i_\mu \to A^i_\mu + \frac{1}{g}\partial_\mu a^i + igf^{ijk}a^j A^k_\mu \tag{2.32}$$

.

The extra term in the gauge field transformation contains the group structure constants f^{ijk} which correspond to the particular group, for example ϵ^{ijk} for SU(2). They are derived from the general commutation formula of the group generators

$$[\tau^i, \tau^j] = if^{ijk}\tau^k \tag{2.33}$$

Additionally, the field tensor needs to be redefined

$$F^i_{\mu\nu} \equiv \partial_\mu A^i_\nu - \partial_\nu A^i_\mu - gf^{ijk}A^j_\mu A^k_\nu \tag{2.34}$$

and transform as

$$F^i_{\mu\nu}\tau^i \to U(x)F^i_{\mu\nu}\tau^i U^\dagger(x) \tag{2.35}$$

or infinitesimally as

$$F^i_{\mu\nu} \to F^i_{\mu\nu} + gf^{ijk}a^j A^j_\mu A^k_\nu \tag{2.36}$$

in order to maintain invariance.

SU(2)

Yang and Mills developed this method utilizing the group SU(2). The generators of this group are the Pauli matrices divided by two

$$\sigma_1 = \begin{pmatrix} 0 & 1 \\ 1 & 0 \end{pmatrix}, \sigma_2 = \begin{pmatrix} 0 & -i \\ i & 0 \end{pmatrix}, \sigma_3 = \begin{pmatrix} 1 & 0 \\ 0 & -1 \end{pmatrix}, \tag{2.37}$$

and the structure constants are the well-known ϵ^{ijk} associated with a vector cross product. The Yang-Mills Lagrangian is the same as the QED Lagrangian, but with the Dirac fields representing two 4-component spinors with color components, 1 or 2

$$\psi = \begin{pmatrix} \psi_1 \\ \psi_2 \end{pmatrix}, \tag{2.38}$$

and the gauge field tensors redefined as above.

$$\mathcal{L}_{Yang-Mills} = i\bar{\psi}\gamma^\mu D_\mu \psi - m\bar{\psi}\psi - \frac{1}{16\pi} F_i^{\mu\nu} F^i_{\mu\nu} \tag{2.39}$$

Unfortunately, the Yang-Mills SU(2) model did not match up with experimental evidence.

SU(3) - QCD

Applying non-Abelian gauge theory to the group known as SU(3) does result in an accurate description of hadronic interactions. SU(3) is the group of 3×3 unitary matrices with determinant of one . In this case, the interaction involves the strong nuclear force and the theory is known as quantum chromodynamics (QCD). The three components (and 3×3 group elements) correlate with the three color types (red, green, and blue) for each quark flavor. The 8 matrices used, SU(3), are known as the Gell-Mann matrices.

$$H = a \cdot \lambda \tag{2.40}$$

$$\lambda_1 = \frac{1}{2}\begin{pmatrix} 0 & 1 & 0 \\ 1 & 0 & 0 \\ 0 & 0 & 0 \end{pmatrix}, \lambda_2 = \frac{1}{2}\begin{pmatrix} 0 & -i & 0 \\ i & 0 & 0 \\ 0 & 0 & 0 \end{pmatrix}, \lambda_3 = \frac{1}{2}\begin{pmatrix} 1 & 0 & 0 \\ 0 & -1 & 0 \\ 0 & 0 & 0 \end{pmatrix},$$

$$\lambda_4 = \frac{1}{2}\begin{pmatrix} 0 & 0 & 1 \\ 0 & 0 & 0 \\ 1 & 0 & 0 \end{pmatrix}, \lambda_5 = \frac{1}{2}\begin{pmatrix} 0 & 0 & -1 \\ 0 & 0 & 0 \\ i & 0 & 0 \end{pmatrix}, \lambda_6 = \frac{1}{2}\begin{pmatrix} 0 & 0 & 0 \\ 0 & 0 & 1 \\ 0 & 1 & 0 \end{pmatrix}, \tag{2.41}$$

$$\lambda_7 = \frac{1}{2}\begin{pmatrix} 0 & 0 & 0 \\ 0 & 0 & -i \\ 0 & -i & 0 \end{pmatrix}, \lambda_8 = \frac{1}{2\sqrt{3}}\begin{pmatrix} 1 & 0 & 0 \\ 0 & 1 & 0 \\ 0 & 0 & -2 \end{pmatrix}$$

The Lagrangian has not changed, but the Dirac fields now represent the 3 color fields for each quark flavor

$$\mathcal{L}_{QCD} = i\bar{\psi}\gamma^{\mu}D_{\mu}\psi - m\bar{\psi}\psi - \frac{1}{16\pi}F_{i}^{\mu\nu}F_{\mu\nu}^{i}\,, \qquad \psi = \begin{pmatrix} \psi_{red} \\ \psi_{blue} \\ \psi_{green} \end{pmatrix} \tag{2.42}$$

The full QCD Lagrangian includes 6 such equations, one for each quark flavor (up, down, charm, strange, top, bottom).

2.2.4 Perturbation and QCD

Now we have a Lagrangian for the nuclear strong force, known as QCD. QCD is the leading theory for the theory of strong interactions. Unfortunately, analytical methods are of limited applicability in the quantized theory. One approach is to expand the action as a Taylor series in terms of the interaction coupling constant. This leads to the Feynman diagram expansion, which only works for small coupling constants. For QED, the coupling constant is $\frac{1}{137}$, so this perturbation method works extremely well. For QCD, this method is only possible at extremely short distances, much less than a Fermi, where the coupling constant is weak and the quarks interact with each other very weakly. This feature of the strong coupling constant is known as asymptotic freedom. As the distance between quarks increases, the coupling constant becomes much stronger, to the point where a Taylor expansion is no longer

valid. In this region, perturbation theory is no longer an option as higher order diagrams yield greater amplitudes and thus divergent results. This stronger coupling region is the region of quark confinement, and so another method is necessary to study quark confinement.

2.2.5 Renormalization

A method known as regularization approaches the problem of divergent integrals in quantum field theory by imposing a cutoff on the upper limit of integrals; the upper limit of infinity in momenta integrals is replaced by the parameter Λ. This parameter represents a momentum cutoff preventing the integral from blowing up. Of course, calculated physical observables need to be independent of the actual value used for Λ if the theory is to be of any value. The coupling constant is dependent on Λ in such a way that calculations of physical observables are unaffected by the particular value of Λ used. For example, the rest energy of a proton is 938 MeV; this value should be obtained whether integrating to a momentum of Λ or 10Λ. The value of the coupling constant at Λ is different than the value at 10Λ, in such a way that both integrals yield the same rest energy of 938 MeV. This coupling constant is referred to as the running coupling constant since its value is energy-dependent, and the procedure of the modification of the coupling constant in such a way to preserve the values of physical observables is known as renormalization.

In practice, in perturbation theory, a naive momentum cutoff is inconsistent with

gauge invariance, so a different procedure known as "dimensional regularization" is used. But the principle is the same; there is a regularization parameter, and the coupling depends on that parameter.

Chapter 3

Lattice Gauge Theory

3.1 Path Integral of the Lattice

The lattice provides a method of regularization known as lattice gauge theory. Space-time is discretized by placing evenly spaced points throughout space-time; the distance between these lattice points provides a natural upper limit to integrals performed in analysis, thereby resulting in convergent integrals. The procedure is done in such a way that gauge invariance is preserved, as outlined below. The path integral of quantum field theory is utilized for calculations on the lattice.

$$Z = \int_{-\infty}^{+\infty} D\phi e^{-i\int d^4x\mathcal{L}} \tag{3.1}$$

In order to simplify extracting values, a rotation is made from time to imaginary time, $t \to it$. The metric is thereby switched from Minkowski to a four-dimensional

Euclidean

$$x^\mu x_\mu = t^2 - \vec{x}^2 \rightarrow x^\mu x_\mu = (it)^2 - \vec{x}^2 = -t^2 - \vec{x}^2 = -x_E^2. \tag{3.2}$$

Rewriting the previous expression for the path integral with a Wick rotation

$$Z = \int_{-\infty}^{+\infty} D\phi e^{-\int d^4 x_E \mathcal{L}_\mathcal{E}} \tag{3.3}$$

the exponent can be seen as a statistical weight (Boltzmann factor) for the fluctuations of ϕ. And so the path integral can be interpreted as the partition function corresponding to the statistical mechanics of a macroscopic system. Note that the Euclidean Lagrangian $\mathcal{L}_\mathcal{E}$ differs from the Minkowski Lagrangian due to the fact that $A_0 \rightarrow -iA_0$. In the case of QED, the Lagrangian changes from $E^2 - B^2$ to $E^2 + B^2$. As lattice spacing is taken to zero (a cutoff at higher energy), the coupling constant, g, of the interaction term is modified (running coupling constant) in order to keep physical observables, such as the mass spectrum, fixed. Attaining the continuum limit by taking the lattice spacing to zero, requires simultaneously taking the limit of the coupling $g \rightarrow 0$.

3.2 Gauge Fields on the Lattice

The links between lattice sites are associated with the gauge fields and assigned members of the SU(N) group

$$U_\mu = e^{iaA_\mu} \tag{3.4}$$

$$A_\mu = A_\mu^i \tau^i \tag{3.5}$$

where A_μ are Hermitian matrices, and U_μ are N×N matrices of determinant 1. The link is unitary; taking the Hermitian conjugate of a link is equivalent to reversing its orientation. The links are represented as $U(n, n+\mu)$, linking the nth lattice point with the $n+\mu$ lattice point, where μ defines one lattice unit in the μ direction.

3.3 The Lattice Action

A plaquette is defined as a (unit) square face of the lattice with dimensions $a \times a$. The action of the lattice is equal to tracing U's around each of the plaquettes of the lattice and summing the real part:

$$S = -\frac{1}{2g^2} \sum_{n,\mu,\nu} \mathrm{Re}\left\{\mathrm{Tr}[U_p]\right\}, \tag{3.6}$$

where

$$U_p = U(n, n+\mu)U(n+\mu, n+\mu+\nu)U(n+\mu+\nu, n+\nu)U(n+\nu, n). \tag{3.7}$$

This formulation is both gauge invariant and reproduces the Yang-Mills theory action in the continuum (lattice spacing goes to zero) limit

$$S \sim \frac{1}{4} \int d^4x F^a_{\mu\nu} F^{\nu\mu a} \tag{3.8}$$

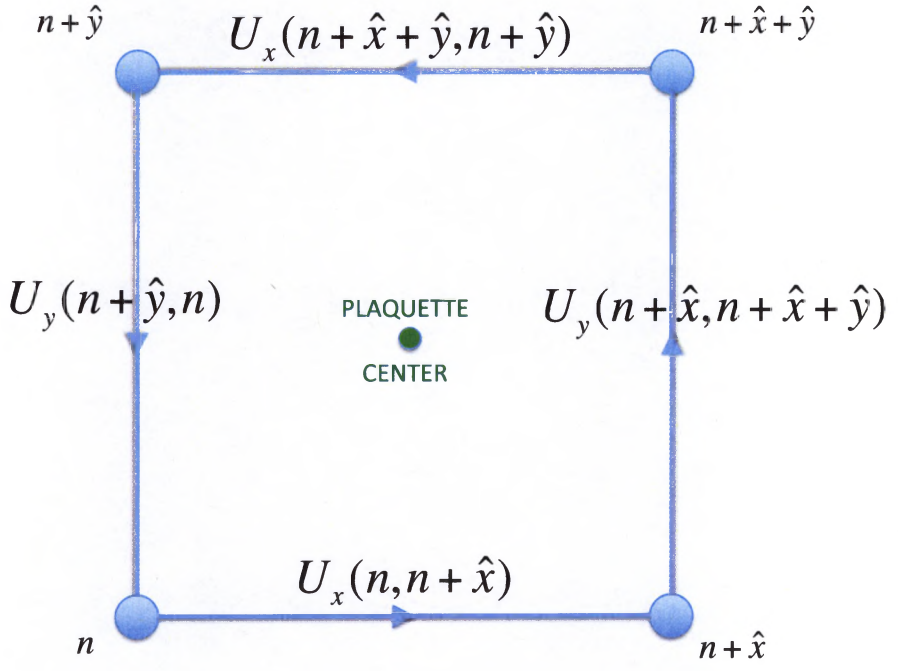

Figure 3.1: Plaquette action

Examining the action of a single plaquette in the xy plane in terms of the gauge

fields as shown in Figure 3.1 we obtain

$$S_{\Box} = -\frac{1}{2g^2}\mathrm{Re}\left\{\mathrm{Tr}[U_x(n, n+\hat{x})U_y(n+\hat{x}, n+\hat{x}+\hat{y})U_x(n+\hat{x}+\hat{y}, n+\hat{y})U_y(n+\hat{y}, n)]\right\}. \tag{3.9}$$

Switching the direction of a link has the effect of replacing each gauge field with its Hermitian conjugate. Therefore, if we reverse the direction of the last two links in the loop, the action can be rewritten as

$$S_{\Box} = -\frac{1}{2g^2}\mathrm{Re}\left\{\mathrm{Tr}[U_x(n, n+\hat{x})U_y(n+\hat{x}, n+\hat{x}+\hat{y})U_x^{\dagger}(n+\hat{y}, n+\hat{x}+\hat{y})U_y^{\dagger}(n, n+\hat{y})]\right\}. \tag{3.10}$$

As stated earlier, a gauge field is assigned to each link

$$U_{\mu} = e^{iaA_{\mu}} \tag{3.11}$$

Thus, rewriting the action in terms of the gauge fields we obtain

$$S_{\Box} = -\frac{1}{2g^2}\mathrm{Re}\left\{\mathrm{Tr}[e^{iaA_x(n,n+\hat{x})}e^{iaA_y(n+\hat{x},n+\hat{x}+\hat{y})}e^{-iaA_x(n+\hat{y},n+\hat{x}+\hat{y})}e^{-iaA_y(n,n+\hat{y})}]\right\}. \tag{3.12}$$

For small lattice spacing a, we can Taylor expand each gauge field about the center of the plaquette.

$$A_x(n, n+\hat{x}) = A_x - \frac{a}{2}\partial_y A_x + \ldots \tag{3.13}$$

$$A_y(n+\hat{x}, n+\hat{x}+\hat{y}) = A_y + \frac{a}{2}\partial_x A_y + \ldots \tag{3.14}$$

$$A_x(n+\hat{y}, n+\hat{x}+\hat{y}) = A_x + \frac{a}{2}\partial_y A_x + \ldots \tag{3.15}$$

$$A_y(n, n+\hat{y}) = A_y - \frac{a}{2}\partial_x A_y + \ldots \tag{3.16}$$

The action now reads

$$S_\Box = -\frac{1}{2g^2}\mathrm{Re}\left\{\mathrm{Tr}[e^{ia(A_x - \frac{a}{2}\partial_y A_x + \ldots)} e^{ia(A_y + \frac{a}{2}\partial_x A_y + \ldots)} e^{-ia(A_x + \frac{a}{2}\partial_y A_x + \ldots)} e^{-ia(A_y - \frac{a}{2}\partial_x A_y + \ldots)}]\right\}. \tag{3.17}$$

Since the gauge fields are linear combinations of group generators, we need to use the Baker-Campbell-Hausdorff (BCH) formula for exponential matrices

$$e^A e^B = e^{A+B+[A,B]/2+\ldots} \tag{3.18}$$

in order to combine the first and second and third and fourth exponents.

$$S_\Box = -\frac{1}{2g^2}\mathrm{Re}\left\{\mathrm{Tr}[e^{ia(A_x + A_y - \frac{a}{2}\partial_y A_x + \frac{a}{2}\partial_x A_y + \frac{ia}{2}[A_x, A_y] + O(a^2))} e^{-ia(A_x + A_y + \frac{a}{2}\partial_y A_x - \frac{a}{2}\partial_x A_y + \frac{ia}{2}[A_x, A_y] + O(a^2))}\right\} \tag{3.19}$$

Applying the BCH formula once again, and dropping terms of order greater than two in a we obtain

$$S_\Box = -\frac{1}{2g^2}\mathrm{Re}\left\{\mathrm{Tr}[e^{ia^2(\partial_x A_y - \partial_y A_x - [A_x, A_y])}]\right\} \tag{3.20}$$

Recognizing the exponent as the gauge field tensor and generalizing to all four

dimensions

$$S_{\square} = -\frac{1}{2g^2}\sum_{\square} \mathrm{Re}\left\{\mathrm{Tr}[e^{ia^2 F_{\mu\nu}}]\right\} \tag{3.21}$$

Expanding the exponent as a Taylor series

$$S_{\square} = -\frac{1}{2g^2}\sum_{\square} \mathrm{Re}\left\{\mathrm{Tr}[1 + ia^2 F_{\mu\nu} + (ia^2 F_{\mu\nu})^2 + \ldots]\right\} \tag{3.22}$$

Since the gauge fields are comprised of linear combinations of Hermitian, traceless matrices, the second term èquals zero. Dropping the constant, as well all terms of order greater than two, the action reduces to

$$S_{\square} = \frac{a^4}{2g^2}\sum_{\square} \mathrm{Tr}[F^{\mu\nu} F_{\mu\nu}] \tag{3.23}$$

Taking the limit of a to zero spacing we obtain the Yang-Mills continuum action.

$$S_{\square} = \frac{1}{2g^2}\int d^4x \mathrm{Tr}[F^{\mu\nu} F_{\mu\nu}] \tag{3.24}$$

Now that we have an action, we need to find gauge invariant quantities since observable quantities are associated with gauge invariant quantities. Previously it was shown that the trace of a plaquette is gauge invariant. In fact, the trace of the product of any rectangular discretized loop on the lattice is gauge invariant and is known as a Wilson loop. A plaquette is essentially the unit Wilson loop. The

continuum version of the Wilson Loop operator is

$$\Phi(C) = P\,\mathrm{Tr}[exp(i \oint_C A_\mu dx^\mu)], \tag{3.25}$$

path ordering (P) of the exponential along a closed continuous loop (C).

3.4 The Wilson Loop

3.4.1 The Static Inter-quark Potential

A measurement (on the lattice) of a rectangular Wilson loop is related to the potential of a static quark-anti-quark pair. Consider a rectangular Wilson loop of size R and T, where R and T refer to the size in lattice units of the planar loop that is being measured on the lattice; for example W(5,3) would refer to a 5×3 rectangular loop. This loop corresponds to the creation of a quark and anti-quark at one T end of the rectangle, the propagation of the pair through time (the T direction on the lattice), and annihilation of the pair at the far T end of the loop (see Figure 3.2). The fact that neither the quark, nor the anti-quark, moves in the R direction corresponds to quarks too massive to move. A chromoelectric flux tube is formed between the quark and anti-quark as they propagate from creation to annihilation. This can be shown by writing the Wilson loop as the quantum mechanical amplitude for the creation and annihilation of a quark and anti-quark in the ground state, $|0\rangle$,

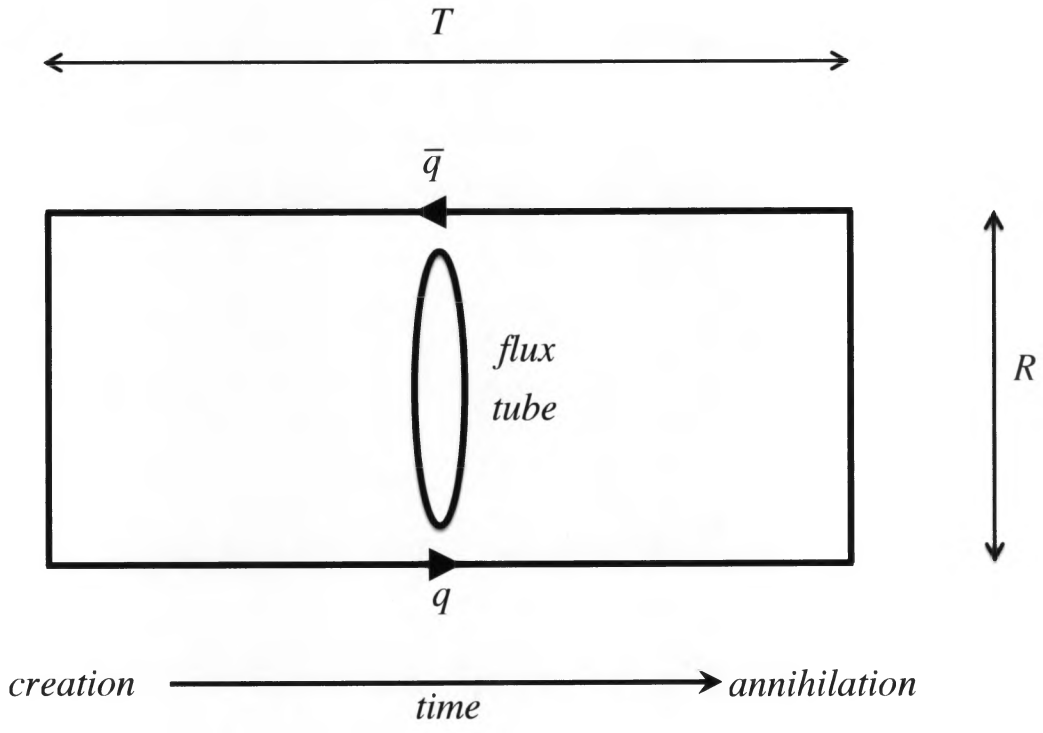

Figure 3.2: Creation and annihilation of static quark and anti-quark.

of the vacuum (in Euclidean time)

$$W(R,T) = \langle 0| Q(t=T)e^{-HT}Q^{\dagger}(t=0) |0\rangle . \tag{3.26}$$

The operator $Q(t)$ represents the creation operator of a two-particle (quark and anti-quark) color-singlet state with separation R

$$Q(t) = \phi^{\dagger}(0,t) \prod_{n=0}^{R-1} U_i^{(r)}(n\hat{i},t)\phi(R\hat{i},t). \tag{3.27}$$

In addition to the two particles, this operator simultaneously also creates the aforementioned color electric flux tube extending between the two particles. Inserting two complete sets of energy eigenstates

$$W(R,T) = \langle 0| Q(T)(\sum_n |n\rangle \langle n|)e^{-HT}(\sum_m |m\rangle \langle m|)Q^{\dagger}(0)|0\rangle \tag{3.28}$$

and noting that

$$\langle n| e^{-HT} |m\rangle = e^{-E_n T}\delta_{mn} \tag{3.29}$$

the amplitude can be written

$$W(R,T) = \sum_n \langle 0| Q(T)|n\rangle e^{-E_n T} \langle n|)Q^{\dagger}(0)|0\rangle \tag{3.30}$$

As T is taken to infinity, the amplitude is dominated by the lowest energy state and the amplitude becomes

$$constant \times e^{-E_{lowest}T} \tag{3.31}$$

where the constant is

$$\langle 0|\, Q(T)\, |lowest\, energy\rangle\, \langle lowest\, energy|\, Q^{\dagger}(0)\, |0\rangle\, . \tag{3.32}$$

The lowest energy corresponds to the interaction potential $V(R)$ (plus the R-independent self-energies), and so the resulting expression for the Wilson loop is

$$lim_{T\to\infty} W(R,T) = constant \times e^{-V(R)T} \tag{3.33}$$

3.4.2 An Indicator of Confinement

The potential between a quark and anti-quark approaches, at large R, the string tension between them multiplied by the distance between them: $V(R) = \sigma R$. In a confining theory, the σ represents the magnitude of the force between the quark and anti-quark; a higher value correlates to a greater force between the two. For a linear potential, σ is the force between the quarks known as the string tension and is extremely important in quark theory. The string tension has been computed numerically via lattice Monte Carlo simulations and its values are well-accepted. In non-Abelian theory, an R×T Wilson Loop oriented along the time axis and one spatial direction provides a method of measuring the non-abelian electric or "color" electric flux flowing through that particular loop. The Wilson Loop can be positive or negative, and averaging over many different values due to vacuum fluctuations can produce an average result that decreases exponentially with the size of the loop.

It has been shown that a Wilson Loop value that decays in a manner that correlates with the area of the loop indicates a theory of confined quarks.

Quark confinement in strong coupling expansions has been proven within the framework of QCD. At weaker couplings, towards the continuum limit, the evidence is fairly compelling, but it comes from lattice Monte Carlo simulations. The criterion for confinement is the area law for the behavior of Wilson loops for large T, W : $W(R,T) \sim e^{-\sigma RT}, RT$ =area. Conversely, non-confining potentials yield a perimeter law for Wilson loops: $W(R,T) \sim e^{-cT}, c = constant$ (large R and T). The area law is related to the linear potential (long distances), as opposed to asymptotic freedom (short distances). Perturbation theory never sees this linear potential, and so we can't use perturbation theory.

3.5 Monte Carlo

Numerical simulations provide a mechanism to measure Wilson Loops as well as other lattice observables. However, it is impossible to sum over all configurations because there is an infinite number of configurations. The Monte Carlo method of simulation attempts to yield a representative sample of configurations of the lattice, similar to thermalized configurations in statistical mechanics. The contribution of the average Wilson Loop of these sample configurations should then provide an accurate estimate of the actual Wilson loop expectation value. By generating hundreds of such configurations on relatively large lattices, measurements should

converge to the correct values according to statistical theory. This is the crux of Monte Carlo method of simulation.

Simulations involve sweeping through all sites of the lattice and using physical probabilities related to energy levels (Boltzmann probabilities) to determine possible values at the links between each lattice site. Links are generated stochastically via Boltzmann probabilities of e^{-S_E}, where S_E is the Euclidean action. These link values are matrix-valued, and this is associated with the fact the quarks (the matter field), and gluons (the force-carrying particles) have a variety of charges (known as "colors"). After a certain number of these probability sweeps have been performed, the algorithm calls for measuring the values of various-sized Wilson Loops throughout the entire lattice and calculating the average Wilson Loop value for each size. The manner in which the Wilson loops decay indicates whether quarks are confined or unconfined. This is the significance of Wilson loop calculations for quark confinement theory.

Chapter 4

Center Vortices

4.1 Center Symmetry

Center vortex theory was introduced by Gerard T'Hooft in 1978 and is closely linked to center symmetry. Center symmetry distinguishes between confining and non-confining potentials, and is therefore an important feature of confinement. If quarks are free, then the center symmetry is broken.

4.1.1 Center of a Group

The center C of a group G is the set of elements of that group that commute with all elements of the group.

$$[C, G] = 0 \tag{4.1}$$

In order to meet this condition for an SU(N) group, C must be proportional to the identity matrix

$$C = e^{i\alpha}\mathbb{1}, \quad \alpha \in [0, 2\pi] \tag{4.2}$$

Additionally, SU(N) requires the determinant of C to equal 1, therefore

$$\det e^{i\alpha}\mathbb{1} = 1 \quad \Rightarrow \quad e^{iN\alpha} = 1 \tag{4.3}$$

and so

$$\alpha_n = \frac{2\pi n}{N}, \quad n = 0, 1, \ldots N-1 \tag{4.4}$$

The center elements for SU(N) may therefore be written

$$z_n \mathbb{1}_N = e^{i2\pi n/N} \begin{pmatrix} 1 & & & 0 \\ & 1 & & \\ & & \ddots & \\ & & & 1 \\ 0 & & & 1 \end{pmatrix} \tag{4.5}$$

The elements $z_n = e^{i2\pi n/N}$ belong to the discrete abelian subgroup Z_N, and the set is the Z_N subgroup of SU(N). In the case of SU(2), the elements are simply 1 and -1.

4.1.2 Center Symmetry and the Lattice Action

Now let's examine how the lattice action is affected by a transformation of the links involving the center subgroup. Let's multiply the timelike links at a fixed time by an element of the center subgroup

$$U_0(\vec{x}, t_0) \rightarrow z U_0(\vec{x}, t_0) \tag{4.6}$$

with $z \in Z_N$ and gauge group SU(N). This is a global transformation, all timelike links are multiplied by the same center element z. The only affected elements of the lattice action are the timelike plaquettes. But these plaquettes are in fact unchanged, due to the fact that the center elements commute with all elements of the group, and therefore with any link variable.

$$P_{i0} = U_i(\vec{x}, t_0) U_0(\vec{x} + \hat{\imath}, t_0) U_i^\dagger(\vec{x}, t_0 + 1) U_0^\dagger(\vec{x}, t_0) \tag{4.7}$$

$$P_{i0} \rightarrow P_{i0}{}' \tag{4.8}$$

$$\begin{aligned} P_{i0}{}' &= U_i(\vec{x}, t_0)\, z\, U_0(\vec{x} + \hat{\imath}, t_0) U_i^\dagger(\vec{x}, t_0 + 1) U_0^\dagger(\vec{x}, t_0)\, z^{-1} \\ &= U_i(\vec{x}, t_0) U_0(\vec{x} + \hat{\imath}, t_0) U_i^\dagger(\vec{x}, t_0 + 1) U_0^\dagger(\vec{x}, t_0)\, z\, z^{-1} \\ &= U_i(\vec{x}, t_0) U_0(\vec{x} + \hat{\imath}, t_0) U_i^\dagger(\vec{x}, t_0 + 1) U_0^\dagger(\vec{x}, t_0) \\ &= P_{i0} \end{aligned} \tag{4.9}$$

Since plaquettes are unaffected by a broken center symmetry, the action and the Wilson loops are also unaffected.

A gauge-invariant observable that is affected by the center symmetry is known as a Polyakov loop. A Polyakov loop is the trace of a line that winds once around the lattice in the periodic time direction.

$$P(\mathbf{x}) = \mathrm{Tr} \prod_{n_t=1}^{L_t} U_0(\mathbf{x}, n_t) \tag{4.10}$$

L_t is the extension of the lattice in the time direction. Since the center transformation affects all timelike links at a *fixed time*, only one of the links in the Polyakov loop will be affected by the transformation. As a result, under the center transformation $U_0(x, t_0) \to zU_0(x, t_0)$, the Polyakov loop transforms as

$$P(\mathbf{x}) \to zP(\mathbf{x}) \tag{4.11}$$

The expectation value of the Polyakov loop therefore serves as an indicator of whether or not the center symmetry is broken.

$$\langle P(\mathbf{x}) \rangle \neq 0 \Rightarrow \textit{broken } Z_N \textit{ symmetry phase} \tag{4.12}$$

Physically, the Polyakov represents a heavy quark sitting still in space while propagating in the time direction on the lattice. Its expectation value can be shown

to be related to the free energy, F_q of an isolated, static quark

$$\langle P(\mathbf{x}) \rangle = e^{-\beta F_q} \tag{4.13}$$

where $\beta = 1/T$ as in statistical mechanics. Additionally, $\beta = L_t a$, where a is the lattice spacing. The above equation reveals that a non-zero expectation value for the Polyakov loop indicates a finite free energy for a quark. Only if the expectation value is zero, corresponding to a phase of unbroken center symmetry, is the free energy infinite. The unbroken center symmetry phase is therefore an indicator of confinement. Conversely, if this center symmetry is broken, then the static quark potential cannot be asymptotically linear and must, in fact, become flat, corresponding to a de-confined phase. Center symmetry is therefore very useful for distinguishing between confined and de-confined phases.

4.2 Center Vortices on the Lattice

4.2.1 Center Vortex Creation

Center vortices are closely associated with center symmetry. Center vortices are line-like topological defects that exist in the vacuum of Yang-Mills theory and quantum chromodynamics. They theoretically represent magnetic vortices, which carry magnetic flux in the center of the gauge group. The effect of creating a center vortex

topologically linked to a given Wilson loop, in an SU(N) gauge theory, is to multiply the Wilson loop by an element of the gauge group center

$$W(C) \to e^{i2\pi n/N} W(C), \qquad n = 1, \ldots, N-1 \tag{4.14}$$

4.2.2 Finding Center Vortices

Finding center vortices on the lattice involves fixing to a gauge which brings link variables as close as possible, on average, to center elements. The gauge fixing procedure is described in detail in Section 5.4. Values of Wilson Loops range continuously from -1 to +1. We can force the links to take a stand in one direction or the other by forcing all positive-valued links to +1 and all negative-valued links to -1. Mathematically we are mapping an $SU(2)$ lattice to a Z_2 lattice, a procedure known as center projection.

Examining the plaquettes on a projected Z_N lattice, a "$P - plaquette$" is defined as a plaquette whose value is any element of the Z_N group other than unity. These P-plaquettes locate the position of excitations on the Z_N lattice known as "$P - vortices$". These P-vortices are the center vortices of Z_N gauge theory, and theoretically they are located somewhere in the middle of the thick center vortices of the original lattice. P-vortices are not actually located on the original lattice, but on a "dual" lattice. The sites of the dual lattice are shifted half a lattice spacing away from the sites of the original lattice. In four dimensions, a P-vortex is a sur-

face comprised of plaquettes which are dual to P-plaquettes. A P-vortex pierces the center of each P-plaquette, carrying magnetic flux in the center of the gauge group.

In fact, string tensions computed on the center-projected lattice scale well, and agree fairly well with the asymptotic string tensions computed on the unprojected lattice. Data from simulations show that center projection effectively removes any Coulombic contribution of the potential for Wilson loops as small as $R = 2$, revealing the confining linear potential associated with the string tension. These same simulations reveal that the Z center variables carry most of the information about the string tension, and are therefore the crucial part of the A links. This phenomenon is referred to as center dominance.

4.2.3 Correlation with Wilson Loop Area Law

In order to understand how center vortices can be correlated with an area law fall-off for the Wilson loop, we can picture a 2-D L×L planar space slice of 4-D space-time with the time direction extended into the page. A total of N vortices piercing the plane and extending in the time direction are represented by dots. A Wilson loop of area A is shown within this plane and is pierced by n vortices. In $SU(2)$ gauge theory, each center vortex contributes a value of -1 to the Wilson loop. If the vortex piercings are uncorrelated, then we can calculate the expectation value for the Wilson loop by summing over all possibilities with binomial weighting and

extending the plane to be infinitely wide so that N goes to infinity

$$\begin{aligned} < W > &= \lim_{N\to\infty} \sum_{n=0}^{N} (-1)^n \binom{N}{n} \left(\frac{A}{L^2}\right)^n \left(1 - \frac{A}{L^2}\right)^{N-n} \\ &= \lim_{N\to\infty} \left(1 - \frac{2A}{L^2}\right)^N \\ &= \lim_{N\to\infty} \left(1 - \frac{2NA}{NL^2}\right)^N \\ &= \lim_{N\to\infty} \left(1 - \frac{2\rho A}{N}\right)^N \\ &= e^{-\rho A} \end{aligned} \tag{4.15}$$

where $\rho = \frac{N}{L^2}$, the vortex density in the plane. The result is an area law for the Wilson loop, consistent with confined quarks. Repeating this calculation in a phase where the vortex piercings are indeed correlated yields a perimeter law for the Wilson loop, therefore indicating a de-confined phase.

Center vortices are the only field configurations which generate string tensions for Wilson loops that depend only on the N-ality of the loop, and which do not have to appeal to some further color-screening mechanism. N-ality is determined by the representation of the group. If $M[g]$ is the matrix representation of group element g in a representation of N-ality k, and $z \in Z_N$ is an element in the center, then

$$M[zg] = z^k M[g] \tag{4.16}$$

Chapter 5

Method

5.1 Overview

We can test the center vortex theory by locating loops which have one center vortex and loops which have no center vortices. We then look at the average Wilson Loop (on the original $SU(2)$ lattice) for loops pierced by one center vortex and compare it with the average Wilson Loop for the loops with no center vortex piercings. Finally, we extrapolate the string tension from the ratios of these values ($W1/W0$) and compare with the value of the known values of the string tension. If center vortex theory is correct, the string tensions taken from different sized-loop and at different lattice couplings should match the known string tensions.

5.2 Lattice creation

The first step was to create a four-dimensional lattice, corresponding to the four dimensions of spacetime, consisting of points (lattice sites) and lines (lattice links) connecting the points. These simulations were done on a lattice of hypervolume of size 24^4, 24 lattice units and 24 lattice links in each dimensional direction. Each link on the lattice is assigned an element of the gauge group $SU(2)$. The inverse of this element is associated with an inverse link, a link between the same two lattice sites but pointing in the opposite direction,

$$U_{ij} = U_{ji}^{-1}, \tag{5.1}$$

for the link located between lattice sites i and j. The $SU(2)$ elements for each link are assigned according to the relation

$$U = a_0 \mathbb{1} + i\vec{a} \cdot \vec{\sigma} \tag{5.2}$$

where a_0 and $\vec{a}$ are the components of a four-vector a^μ, $\mathbb{1}$ is the 2×2 identity matrix, and $\vec{\sigma}$ corresponds to the three Pauli matrices.

In order to satisfy the constraint

$$a_0^2 + \vec{a} \cdot \vec{a} = 1 \tag{5.3}$$

the components of a_μ are randomly assigned in a "hot start" as follows:

$$\begin{aligned} -1 \leq a_0 \leq 1 \\ -1 \leq b \leq 1 \\ a_3 = b\sqrt{1 - a_0^2} \\ 0 \leq \phi \leq 2\pi \\ a_1 = \cos\phi\sqrt{(1 - (a_0)^2 - (a_3)^2} \\ a_2 = \sin\phi\sqrt{(1 - (a_0)^2 - (a_3)^2} \end{aligned} \tag{5.4}$$

For the link from lattice site i to site j, the inverse link from j to i is assigned the following four-vector values:

$$\begin{aligned} (a_0)_{ji} = (a_0)_{ij} \\ (\vec{a})_{ji} = -\vec{a}_{ij} \end{aligned} \tag{5.5}$$

These values ensure that the length of each four-vector is equal to one, and that the matrix associated with the inverse link is indeed the inverse of the matrix of the forward link.

5.3 Creutz Heat Bath

Now that all links have been assigned an element of the gauge group $SU(2)$, each link on the lattice is successively subjected to a statistical heat bath. This has the

effect of simulating a state of thermal equilibrium. The element, U_{ij}, associated with each link is replaced with a new element, U'_{ij}, chosen randomly from the group with probability density proportional to the Boltzmann factor,

$$dP(U') \sim e^{-\beta S(U')} dU' \tag{5.6}$$

The action $S(U')$ is evaluated with the given link having value U'_{ij} while maintaining all other links at their previous values.

The first step of the heat bath is to find a new a_0 for the link being subjected to the heat bath. The components of $\vec{a}$ are then found as above. In order to find a new a_0, 6 loops connected to the link are examined. Each link is connected to an up loop and a down loop in each of the three planes perpendicular to the link receiving the heat bath (2 loops per plane $\times$ 3 planes = 6 calculations). The next step is to multiply the three links across each loop and sum the 6 results:

$$\tilde{U} = \sum_{\alpha=1}^{6} (U_{ij} U_{jk} U_{kl})_\alpha \tag{5.7}$$

Next, the determinant of this sum is calculated:

$$k = \sqrt{|\tilde{U}|} \tag{5.8}$$

The possible new a_0 is then randomly assigned the value :

$$\begin{aligned} 0 \leq\ & r_1 \leq 1 \\ r_2 =\ & (1 - r_1)e^{-2\beta k} \\ a_0 =\ & 1 + \ln[r_1 + r_2] \end{aligned} \tag{5.9}$$

This new a_0 is then rejected with the probability of

$$1 - \sqrt{1 - a_0^2} \tag{5.10}$$

This process is repeated until a new value of a_0 is not rejected. The link is then replaced by the product

$$U' = U\bar{U}^{-1} \tag{5.11}$$

where U is assigned the new values for a, and $\bar{U}$is equal to $\tilde{U}/k$.

5.4 Gauge fixing / Center projection

Now that the lattice is in thermal equilibrium, we would like to locate center vortices. This is done by fixing a gauge which reduces the full $SU(2)$ gauge symmetry to the center subgroup Z_2. As mentioned earlier in section 4.2.2, this is known as center projection and maps the full gauge field configuration $U_\mu(x)$ onto configuration $Z_\mu(x) = \pm 1$. The excitations of a Z_2 gauge field are thin center vortices, and

these are used to locate thick center vortices in the full, unprojected gauge field configuration, $U_\mu(x)$.

We start by making a copy of the thermalized lattice. The original lattice is left untouched while all following gauge fixing steps are applied to this lattice copy. Gauge fixing is done utilizing the direct maximal center gauge. This gauge brings the full link variables U as close as possible the the center elements $\pm\mathbb{1}$, by maximizing the quantity

$$R = \sum_{x,\mu} \mathrm{Tr}[U_\mu(x)]^2. \tag{5.12}$$

Sweeping through the lattice, at each site x, we find the gauge transformation g which maximizes the local quantity

$$R_x = \frac{1}{4}\left\{ \sum_{\mu} \mathrm{Tr}[g(x)U_\mu(x)]^2 \; + \; \sum_{\mu} \mathrm{Tr}[U_\mu(x-\hat{\mu})g^\dagger(x)]^2 \right\} \tag{5.13}$$

where

$$g(x) = g_0 I - i\vec{g}\cdot\vec{\sigma} \tag{5.14}$$

$$U_\mu(x) = d_0(\mu)I + i\vec{d}(\mu)\cdot\vec{\sigma} \tag{5.15}$$

$$U_\mu(x-\hat{\mu}) = d_0(\mu+4)I + i\vec{d}(\mu+4)\cdot\vec{\sigma} \tag{5.16}$$

And so R_x reduces to

$$R_x = \frac{1}{2}\sum_{l=1}^{8}\left[\sum_{k=1}^{4} g_k d_k(l)\right]^2 \tag{5.17}$$

In order to maximize the quantity subject to the constraint that g is unitary, we introduce a Lagrange multiplier

$$\tilde{R} = R_x + \frac{1}{2}\lambda\left(1 - \sum_{k=1}^{4} g_k^2\right) \tag{5.18}$$

Differentiating $\tilde{R}$, we find the conditions for a maximum satisfying the constraint

$$\sum_{j=1}^{4}\sum_{l=1}^{8} d_i(l)d_j(l)g_j = \lambda g_i \tag{5.19}$$

$$\sum_{k=1}^{4} g_k^2 = 1 \tag{5.20}$$

This can be written as an eigenvalue equation

$$D\vec{G} = \lambda\vec{G}, \tag{5.21}$$

where

$$D_{ij} = \sum_{l=1}^{8} d_i(l)d_j(l) \tag{5.22}$$

and the unitary constraint is the normalization condition

$$\vec{G}\cdot\vec{G} = 1. \tag{5.23}$$

Finding g now involves finding the eigenvectors of a 4×4 real symmetric matrix.

The eigenvector associated with the largest eigenvalue corresponds to the gauge transformation g maximizing R_x at site x. We sweep through the lattice thousands of times applying the gauge transformation

$$U_\mu(x) \rightarrow g(x)U_\mu(x). \tag{5.24}$$

at each site. The transformation sweeps are stopped once the lattice average of $(\frac{1}{2}\mathrm{Tr}U)^2$ changes by less then 1E-20 after 50 gauge fixing sweeps. Once the criterion is met, a Z_2 lattice is created where

$$Z_\mu(x) = sign[\mathrm{Tr}U_\mu(x)]. \tag{5.25}$$

5.5 P-vortices

Now we search for plaquettes on the projected Z_2 lattice that have a Wilson loop value of -1. Such plaquettes are known as "$P-plaquettes$" and are said to be pierced by "thin" center vortices known as "$P-vortices$". Locating the thin center vortices on the projected Z_2 lattice should help locate thick center vortices on the unprojected $SU(2)$ lattice.

We can test this correlation by taking the following steps. Search the Z_2 lattice for all Wilson loops (of any size, ie, 3×3 links) that have n plaquettes pierced by a thin center vortex. Assign the corresponding Wilson loops on the unprojected

lattice to the ensemble W_n. Search the Z_2 lattice for all Wilson loops with zero plaquettes pierced by center vortices. Assign the corresponding Wilson loops on the unprojected lattice to the ensemble W_0. On the unprojected lattice, calculate the averages for W_n and W_0 for a range of loop sizes and plot the ratio of W_n/W_0 vs loop size. If the P-vortices on the projected Z_2 lattice do indeed locate center vortices on the unprojected $SU(2)$ lattice, then we should expect, asymptotically, that

$$\frac{W_n(C)}{W_0(C)} \rightarrow (-1)^n \tag{5.26}$$

From this relation, we would also expect, asympototically, that

$$\frac{W_{ODD(C)}}{W_{EVEN(C)}} \rightarrow (-1) \tag{5.27}$$

We also note whether the thin center vortex is located in the inner, middle, or outer ring of the Wilson loop. Figures 5.1 and 5.2 show the convention used for labeling the P-plaquette positions "inner", "middle", or "outer". Lastly we search for Wilson loops with center vortices just outside the loop; a P-plaquette bordering the perimeter just outside the loop (and in the plane of the loop), is referred to as "outside".

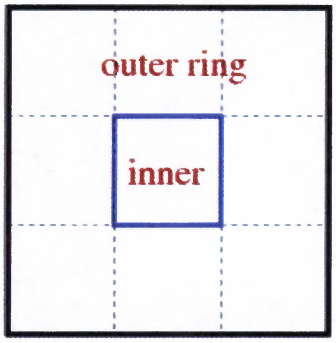

Figure 5.1: Conventions for labeling P-plaquette positions shown for a 3x3 loop

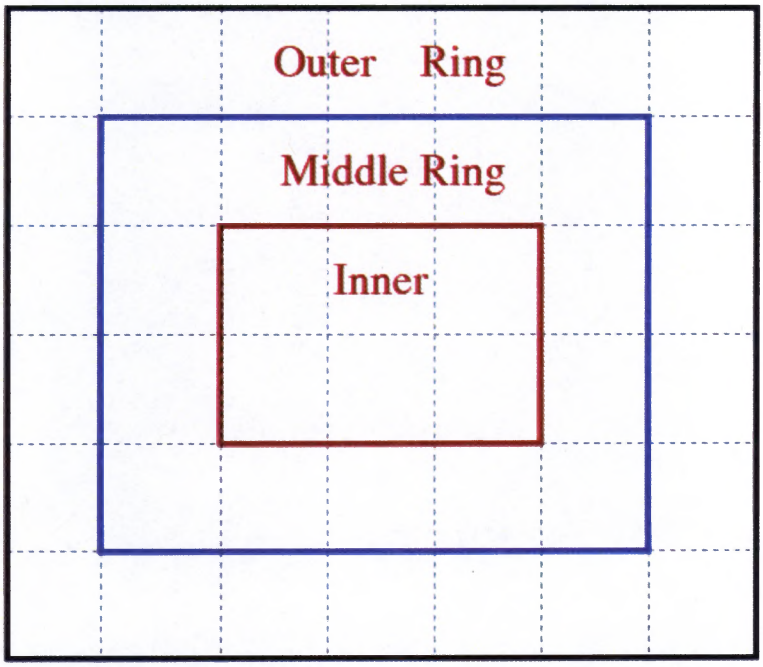

Figure 5.2: Conventions for labeling P-plaquette positions shown for a 7x6 loop

Chapter 6

Results

The first plot involves the ratio of values of $SU(2)$ Wilson loops on the unprojected lattice, linked to a single P-vortex, to that of Wilson loops which are not linked to any P-vortices. These ratios are plotted versus loop area, in physical units, for a range of lattice couplings. For a Wilson Loop of size I by J lattice units, the area in physical units is simply IJa^2, where a is the lattice spacing in physical units. The value for a is β-dependent and is assigned a value at each β that keeps the string tension at its accepted value of (440 MeV)^2.

$$\sigma_{accepted} = \frac{\sigma_{Lattice}}{a^2} \tag{6.1}$$

$$\Rightarrow a = \frac{\sqrt{\sigma_{Lattice}}}{440MeV} \tag{6.2}$$

The value for $\sigma_{Lattice}$ varies with β via the relation

$$\sigma_{Lattice} = e^{13.36-6.68\beta} \tag{6.3}$$

This relation is obtained by taking known values of $\sigma_{Lattice}$ at $\beta = 2.30$, 2.40, and 2.50 and fitting them to the relation

$$\sigma_{Lattice} = e^{A-B\beta} \tag{6.4}$$

Finally, to obtain the loop area in square Fermi, I then used the conversion relation

$$1 \text{ Fermi} = \frac{1}{197 \text{ MeV}} \tag{6.5}$$

As shown in Figure 6.1, the ratios fall approximately on a single curve, consistent with scaling. They also appear to be heading toward the theoretical limit of -1 as the loop area is increased.

The second plot involves the ratio of values of $SU(2)$ Wilson loops on the unprojected lattice, linked to an odd number of P-vortices, to those of Wilson loops linked to an even number of P-vortices. As shown in Figure 6.2, these ratios also fall approximately on a single curve, consistent with scaling. They also appear to be heading toward the theoretical limit of -1 as the loop area is increased.

An unexpected result was a lack of dependence of the ratios on the location

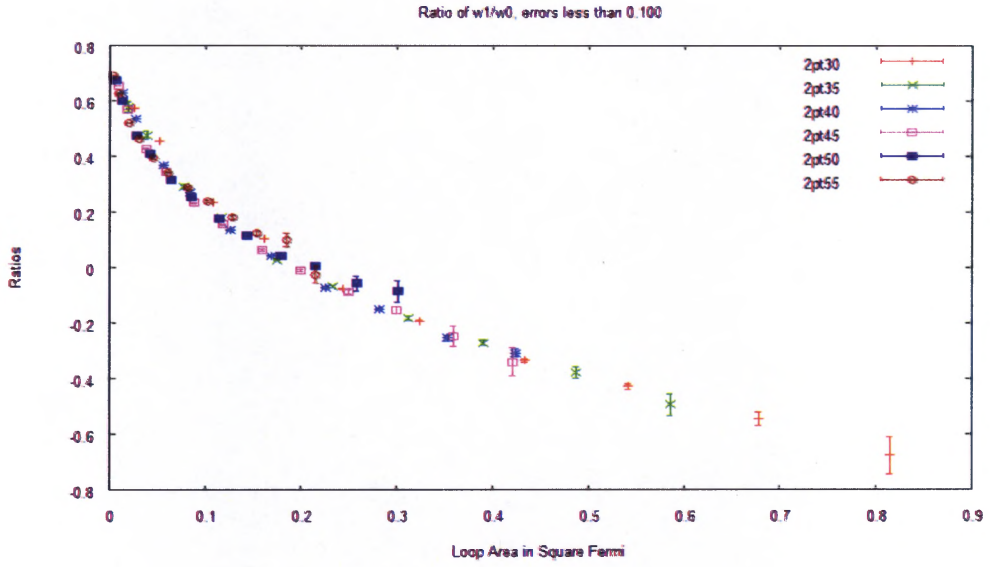

Figure 6.1: Scaling of Wilson Loops Pierced by P-vortices

within the loop of the vortex piercing. Figures 6.2 and 6.3 show plots of the same ratios versus loop area for two different lattice couplings, based on the location of the vortex within the Wilson loop. If a vortex is just outside the Wilson loop, then the ratio is 1, as expected. However, if the ratio appears to be negligibly affected by whether the vortex is located on inner, middle, or outer ring. In other words, the ratios are rather insensitive to the point where the minimal area of the loop is pierced by the P-vortex.

In conclusion, P-vortices are extremely effective at indicating whether center vortices are located inside or outside a Wilson loop, but they are unable to indicate where the center of the center vortex is located.

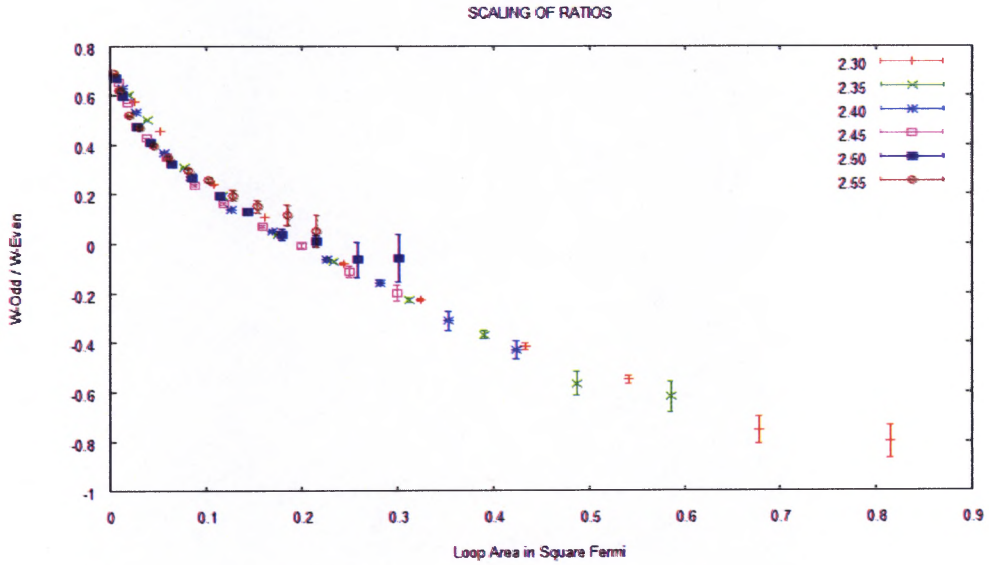

Figure 6.2: Scaling of Odd to Even Wilson Loops

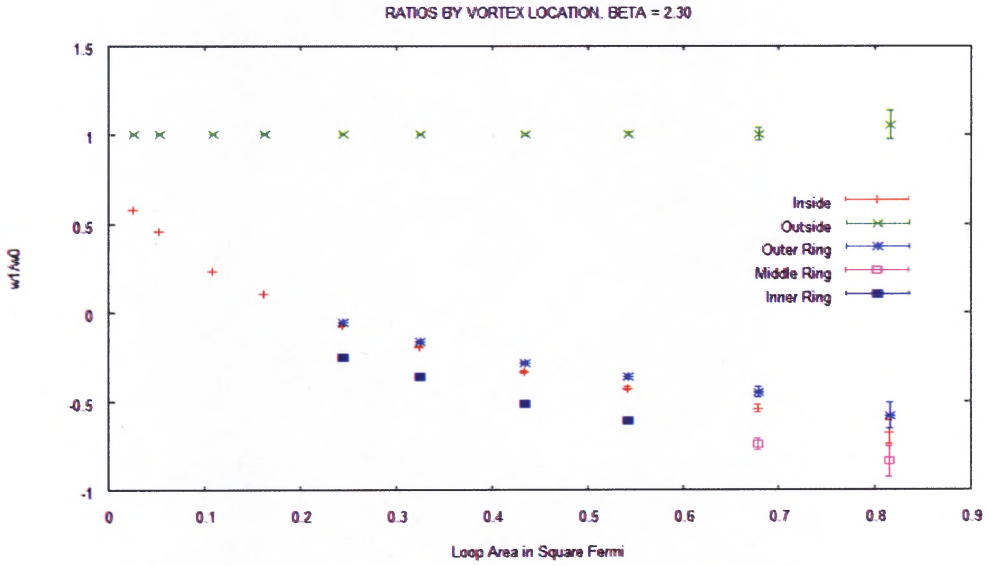

Figure 6.3: Scaling of Wilson Loops by Vortex Location, Beta = 2.30

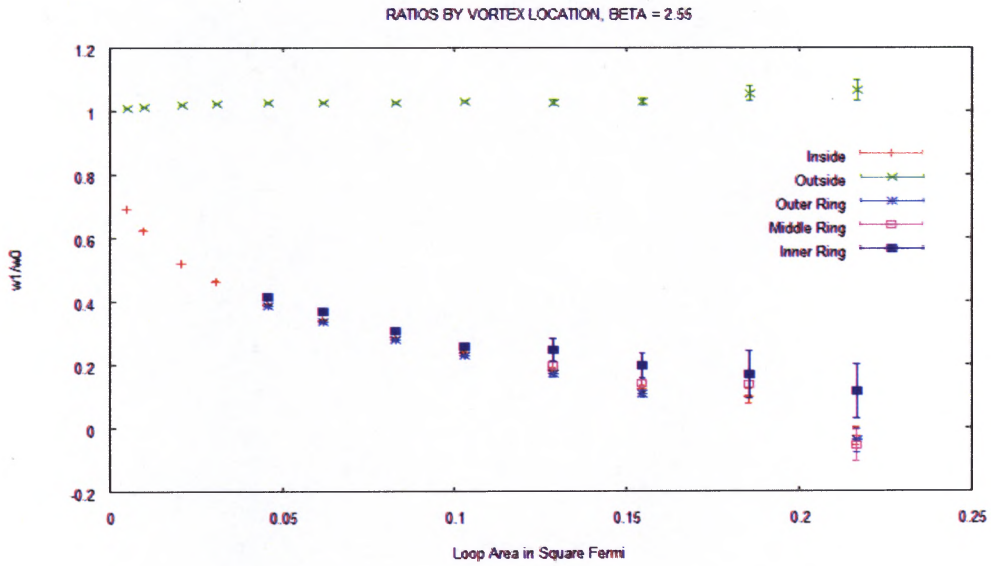

Figure 6.4: Scaling of Wilson Loops by Vortex Location, Beta = 2.55

Bibliography

[1] Michael Creutz. Monte Carlo Study of Quantized SU(2) Gauge Theory. *Phys. Rev.*, D21:2308–2315, 1980.

[2] Michael Creutz. *Quarks, gluons and lattices.* Cambridge Monographs on Mathematical Physics. Cambridge Univ. Press, Cambridge, UK, 1985.

[3] Michael Creutz. The lattice and quantized Yang-Mills theory. In *International Conference on 60 Years of Yang-Mills Gauge Field Theories Singapore, Singapore, May 25-28, 2015*, 2015.

[4] Michael Creutz. Asymptotic Freedom Scales. *Phys. Rev. Lett.*, 45:313, 1980.

[5] Michael Creutz, Laurence Jacobs, and Claudio Rebbi. Monte Carlo Study of Abelian Lattice Gauge Theories. *Phys. Rev.*, D20:1915, 1979.

[6] Luigi Del Debbio, Manfried Faber, Joel Giedt, Jeff Greensite, and Štefan Olejník. Detection of center vortices in the lattice Yang-Mills vacuum. *Phys. Rev.*, D58:094501, 1998.

[7] Luigi Del Debbio, Manfried Faber, Jeff Greensite, and Štefan Olejník. Center dominance, center vortices, and confinement. In *New developments in quantum field theory. Proceedings, NATO Advanced Research Workshop, Zakopane, Poland, June 14-20, 1997*, pages 47–64, 1997.

[8] Patrick Dunn and Jeff Greensite. Scaling properties of Wilson loops pierced by P-vortices. *Phys. Rev.*, D85:097501, 2012.

[9] Michael Engelhardt. Generation of confinement and other nonperturbative effects by infrared gluonic degrees of freedom. *Nucl. Phys. Proc. Suppl.*, 140:92–105, 2005.

[10] Jeff Greensite. An introduction to the confinement problem. *Lect. Notes Phys.*, 821:1–211, 2011.

[11] Jeff Greensite. Center vortices, and other scenarios of quark confinement. *Eur. Phys. J. ST*, 140:1–52, 2007.

[12] Jeff Greensite. The confinement problem in lattice gauge theory. *Prog. Part. Nucl. Phys.*, 51:1, 2003.

[13] Walter Greiner, Stefan Schramm, and Eckart Stein. *Quantum chromodynamics.* Springer, 2002.

[14] David Griffiths. *Introduction to elementary particles.* Wiley-VCH, 2008.

[15] Michael E. Peskin and Daniel V. Schroeder. *An Introduction to quantum field theory.* Addison-Wesley, 1995.

[16] Jan Smit. *Introduction to quantum fields on a lattice.* Cambridge University Press, 2002.

[17] Mark Srednicki. *Quantum field theory.* Cambridge University Press, 2007.

Appendix A: Publication in Phys Rev D

PHYSICAL REVIEW D **85,** 097501 (2012)

Scaling properties of Wilson loops pierced by P-vortices

Patrick Dunn

Physics and Astronomy Department, San Francisco State University, San Francisco, California 94132, USA

Jeff Greensite

*Niels Bohr International Academy, Blegdamsvej 17, DK-2100 Copenhagen Ø, Denmark**

(Received 8 March 2012; published 15 May 2012)

P-vortices, in an SU(N) lattice gauge theory, are excitations on the center-projected Z_N lattice. We study the ratio of expectation values of SU(2) Wilson loops, on the unprojected lattice, linked to a single P-vortex, to that of Wilson loops which are not linked to any P-vortices. When these ratios are plotted versus loop area in physical units, for a range of lattice couplings, it is found that the points fall approximately on a single curve, consistent with scaling. We also find that the ratios are rather insensitive to the point where the minimal area of the loop is pierced by the P-vortex.

DOI: 10.1103/PhysRevD.85.097501 PACS numbers: 11.15.Ha, 12.38.Aw

I. INTRODUCTION

The center vortex theory of confinement [1–6] is motivated by the fact that the asymptotic string tension associated with Wilson loops in group representation r, in a pure SU(N) gauge theory, depends only on the N-ality of that representation, i.e. on the transformation properties of the Wilson loop holonomy with respect to the Z_N center subgroup. This behavior can be understood in "particle" language; e.g. the string which forms between a quark and antiquark in the adjoint representation of the gauge group is eventually broken by pair production of gluons, each of which binds to one of the quarks, resulting in two color singlet states consisting of a quark or antiquark bound to a gluon. This explains why a zero N-ality loop (such as a Wilson loop in the adjoint representation) will have a vanishing asymptotic string tension. On the other hand, there should also be an explanation purely in "field" language, i.e. the dependence on N-ality ought to be explicable in terms of the field configurations which dominate the Euclidean functional integral at very large scales. Such field configurations must be organized in such a way that they generate string tensions for Wilson loops that depend only on the N-ality of the loop. To the authors' knowledge, center vortices are the only field configurations thus far proposed which have this property, and which do not have to appeal to some further color-screening mechanism in the particle picture.

There is a great deal of lattice Monte Carlo evidence in favor of the center-vortex mechanism that has accumulated over the years, cf. the reviews in Refs. [7,8], which mainly cover the SU(2) case, and also the recent work in [9] for the SU(3) gauge group. This data is based on the procedure of center projection in maximal center gauge. One fixes to a gauge (direct- or indirect-maximal center gauge [10]) which brings the link variables as close as possible, on average, to center elements. In the direct-maximal center gauge, the procedure is to maximize

$$R = \sum_{x,\mu} \mathrm{Tr}[U_\mu(x)]\,\mathrm{Tr}[U_\mu^\dagger(x)] \tag{1}$$

via a relaxation technique which reaches a local maximum. This can be regarded as fixing to Landau gauge in the adjoint representation. Link variables $U_\mu(x)$ are then projected to the center element $z_\mu(x) \in Z_N$, which is nearest to $U_\mu(x)$ in the sense that

$$\begin{aligned}&\mathrm{Tr}[(U_\mu(x) - z_\mu(x)\mathbb{1}_N)(U_\mu^\dagger(x) - z_\mu^\dagger(x)\mathbb{1}_N)] \\ &\quad = 2N - \mathrm{Tr}[z_\mu(x)U_\mu^\dagger(x) + h.c]\end{aligned} \tag{2}$$

is minimized. This mapping of configurations $U_\mu(x) \to z_\mu(x)$ from the SU(N) lattice to a Z_N lattice is known as "center projection." String tensions computed on the center-projected lattice, in SU(2) lattice gauge theory, are known to have excellent scaling properties and agree fairly well with the asymptotic string tensions computed on the unprojected lattice, a feature known as "center dominance."[1] The excitations on the projected Z_N lattice are known as "P-vortices." We define a P-plaquette as a plaquette on the projected lattice whose value is an element of the Z_N group different from unity. P-vortices, in D-dimensions, are $D-2$-dimensional objects on the dual lattice, composed of elements (sites, links, or plaquettes in $D = 2$, 3, 4, respectively) which are dual to P-plaquettes. These are the center vortices of a Z_N gauge theory. The value of a Wilson loop on the projected lattice is simply unity times the product of P-plaquettes in the minimal area of the loop.

The question is whether the location of P-plaquettes in the center-projected lattice is correlated to the value of

*Permanent address: Physics and Astronomy Department, San Francisco State University, San Francisco, CA, 94132, USA

[1]There are still some ambiguities, connected with Gribov copies, which can affect this result, cf. [8] for a discussion.

gauge-invariant Wilson loops on the unprojected lattice. The evidence in favor of such a correlation is based on the measurement of "vortex-limited" Wilson loops. A vortex-limited Wilson loop, $W_{n_1,n_2,\ldots n_{N-1}}(C)$, is the expectation value of all loops on the unprojected lattice of shape C whose minimal area contains, on the projected lattice, exactly n_k P-plaquettes equal to center element $z_k = \exp[2\pi ik/N]$, for $k = 1, \ldots, N-1$. In the center vortex picture, if we assume that the thick center vortices do not overlap the loop boundary, then the effect of the center vortices would be to contribute an overall phase factor

$$z = \prod_{k=1}^{n-1} z_k^{n_k} \tag{3}$$

to the value of the loop. The area-law falloff would be due to fluctuations in this phase factor, corresponding to fluctuations in the number of center vortices that are topologically linked to the loop. In this article we will only be concerned with SU(2) lattice gauge theory, where there is only one type of center vortex, and the vortex-limited Wilson loops are denoted $W_n(C)$. The minimal areas of loops contributing to $W_n(C)$ are said to be "pierced" by n P-vortices. We may also define $W_{odd(even)}(C)$ as the expectation value for Wilson loops pierced by an odd (even) number of P-vortices. It was shown in the early work [10] on this subject that W_n depends very strongly on n, and the numerical evidence suggests that in the limit of large loop area

$$\frac{W_n(C)}{W_0(C)} \to (-1)^n \quad \text{and} \quad \frac{W_{odd}(C)}{W_{even}(C)} \to -1. \tag{4}$$

This is consistent with the idea that a P-plaquette on the projected lattice is roughly correlated with the location of a thick center vortex on the unprojected lattice, and that a thick center vortex, if topologically linked to loop C, will contribute a factor of -1 to the loop holonomy. It should be noted that numerical simulations have also shown [10] that vortex-limited Wilson loops $W_0(C)$, $W_{even}(C)$ do not, by themselves, have an area-law falloff, and given that the ratios (4) are of $O(1)$, this lack of area-law falloff must also hold true for $|W_1(C)|$, $W_2(C)$, $|W_{odd}(C)|$. For this reason, it is likely that this absence of area-law falloff holds true in general for all the vortex-limited Wilson loops. The standard Wilson loop expectation value is related to the vortex-limited loops via

$$W(C) = \sum_n p_n(C) W_n(C), \tag{5}$$

where $p_n(C)$ is the probability that the minimal area of a given planar loop C contains n P-plaquettes on the projected lattice. If the $|W_n(C)|$ all have a perimeter-law falloff, as the numerical evidence suggests, then the area-law can only be obtained from cancellations due to the sign differences among the different W_n's, in complete accordance with the center vortex picture.

In the early SU(2) work, the ratio $W_n(C)/W_0(C)$ was only computed at a lattice coupling of $\beta = 2.3$. There was no effort to test scaling, i.e. to check whether the Wilson-loop ratios plotted versus area in physical units fall on a universal curve. In a more recent study, Langfeld [11] investigated the phase of vortex-limited Wilson loops in SU(3) lattice gauge theory at two lattice couplings $\beta = 5.6, 5.8$ and obtained results which were roughly consistent with scaling. In this article we will continue to work with SU (2) loop ratios, as in the early work, but display a larger data set of loop areas at six different lattice couplings, which may give an improved sense of the scaling properties.

II. W_1/W_0 SCALING, AND P-PLAQUETTE LOCATION

Let $W_n[I, J]$ represent the expectation value of a vortex-limited loop, where the loop is a rectangular contour of I lattice units on one side and J lattice units on the other. We will consider loops where $I = J$ and $|I - J| = 1$. The area of the loop in physical units is IJa^2, where the lattice spacing is given, as usual, by $a = \sqrt{\sigma_L/\sigma}$, where σ_L is the string tension in lattice units, and we take $\sigma = (440\ \text{MeV})^2$. Figure 1 displays our results for $W_1[I, J]/W_0[I, J]$ vs area IJa^2 in units of fm^2, for lattice couplings ranging from $\beta = 2.3$ to $\beta = 2.55$ on 24^4 lattice volumes. The data seems to fall roughly on the same curve, which indicates that the W_1/W_0 ratio is a physical observable of some kind. The usual interpretation of these results is that a single P-plaquette found on the projected lattice, in the minimal area of loop C, indicates that loop C is linked to a thick center vortex on the unprojected lattice. Of course, a small loop on the unprojected lattice cannot be affected by the full center flux carried by a thick center vortex, so one does not expect $W_1(C)/W_0(C)$ to equal -1 in that case. This limit should be obtained, however, when the loop area grows much larger than the cross-sectional

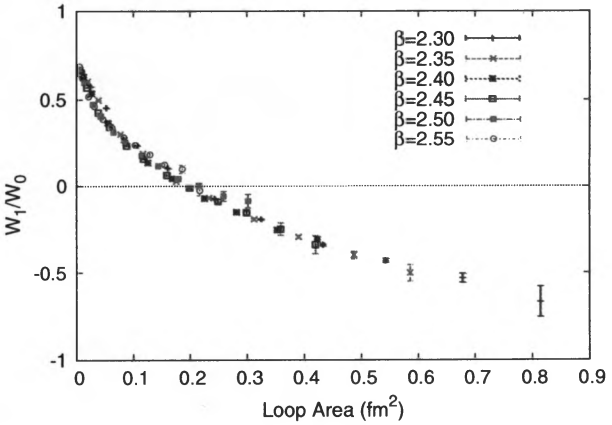

FIG. 1 (color online). Ratio of vortex-limited Wilson loop expectation values $W_1(C)/W_0(C)$ vs loop area in physical units at various lattice couplings.

area of a vortex, so the single vortex linked to the loop does not overlap the boundary of the loop. Figure 1 appears to be consistent with this expectation, although only for the lowest couplings are we able to measure loops which are large enough, in physical units, such that the W_1/W_0 ratio approaches the expected asymptotic value of -1.

We next consider the question of how the ratio $W_1(C)/W_0(C)$ depends on the position of the P-plaquette within the minimal area of loop C. For this study we will also consider the case, which does not really belong to W_1, in which the P-plaquette lies in the plane of loop C but just outside the minimal area, bordering the perimeter of loop C. The ratio of Wilson loops of this kind to W_0 will be represented by data points labeled "outside." Points labeled "inside" are the usual ratios of W_1/W_0. We then make the following distinctions: Consider all plaquettes inside the minimal area of the loop, which border the perimeter. These plaquettes belong to the minimal area bordered by C and another rectangular loop C_1. If the minimal area of C_1 is nonzero, then the data for W_1/W_0 with P-plaquettes in this region between C and C_1 is labeled "outer ring." Next, consider P-plaquettes in the minimal area of C_1 bordering the perimeter of C_1 and another rectangular loop C_2. If the minimal area of C_2 is nonzero, these P-plaquettes belong to the "middle ring," and any P-plaquettes within the minimal area of C_2 are denoted "inner." If, on the other hand, the minimal area of C_2 is zero, then P-plaquettes in the minimal area of C_1 are themselves denoted "inner." Our conventions are illustrated in Fig. 2.

The numerical results shown for $\beta = 2.3$ in Fig. 3 and $\beta = 2.55$ in Fig. 4 are a little surprising, since one would expect that if the location of a P-vortex were strongly correlated with the middle of a thick center vortex, then the ratio $W_1(C)/W_0(C)$, for a large loop, would systematically fall from outer to middle to inner. While this does seem to be true at $\beta = 2.3$, it is not a very large effect and is not observed at all at $\beta = 2.55$ (if anything, the expected order is reversed). The really striking effect is the dramatic dependence on whether a P-plaquette lies just outside, or just inside, the perimeter of the loop. If the P-plaquette lies just outside the loop (data points labeled "outside"), then the expectation value of the loop differs hardly at all from W_0. In sharp contrast, if the P-plaquette lies anywhere within the minimal area of the loop, including at the loop perimeter, then the loop expectation value differs greatly from W_0. This difference between loops with one inside P-plaquette at the perimeter and loops with one outside P-plaquette at the perimeter increases with loop area, and it is quite remarkable in view of the insensitivity of W_1/W_0 to the location of the P-plaquette within the minimal area.

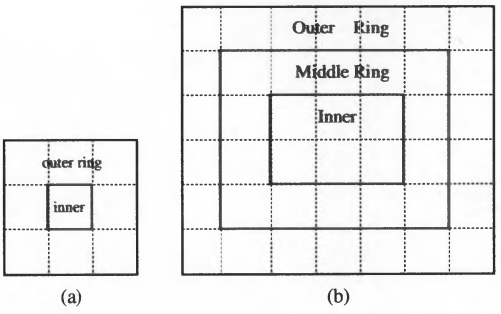

FIG. 2 (color online). Conventions for labeling P-plaquette positions. Plaquettes in the plane of, but just outside the loop, bordering the perimeter, are referred to as "outside."

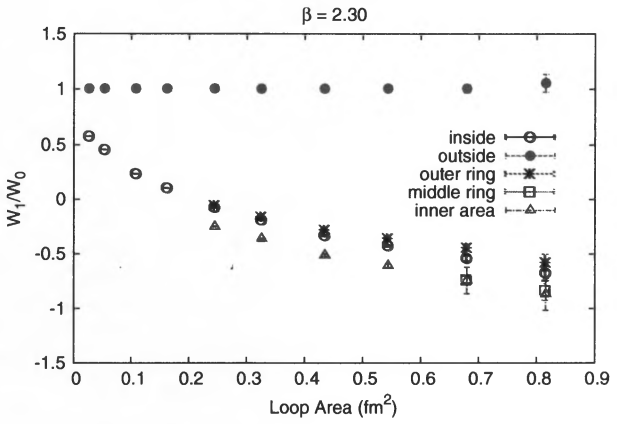

FIG. 3 (color online). Vortex-limited Wilson loop ratios vs loop area in physical units, for specific positions of the P-vortex relative to the loop perimeter (see Fig. 2) at $\beta = 2.3$.

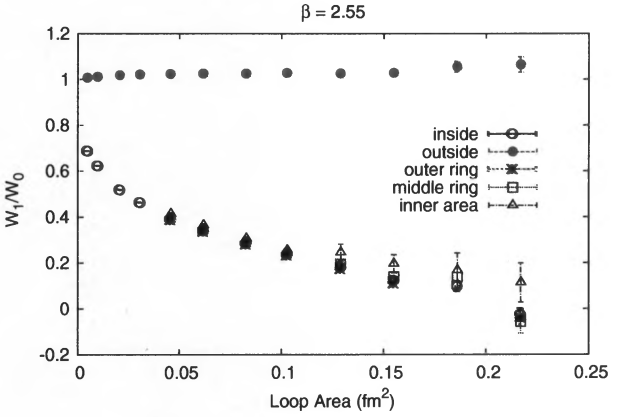

FIG. 4 (color online). Same as Fig. 3 at $\beta = 2.55$.

III. DISCUSSION

We have seen that the $W_1(C)/W_0(C)$ ratio scales reasonably well with β, and also that there is an extremely strong correlation between the expectation value of a Wilson loop, and whether a P-plaquette, bordering the perimeter, lies just inside or just outside the minimal area. There are *a priori* reasons to expect the scaling property, since, e.g., center-projected string tensions scale rather nicely [10], but such a strong distinction between P-plaquettes lying just

inside or just outside the loop is a little surprising, especially for large loops at large β. For a thick center vortex, one would expect that the amount of center flux penetrating the minimal area of the loop would not be very different if the middle of the vortex were located just inside, or just outside, the loop perimeter. Yet the trend of our data indicates that expectation values of large loops depend very strongly on whether or not a single P-plaquette is located inside the loop, but, if inside, the loop expectation value is rather insensitive to exactly *where* inside. This result would make perfect sense if P-vortices were very strongly correlated with the position of center vortices on the unprojected lattice, and if those center vortices were only one lattice spacing wide. But if that were the case, then the ratio $W_1(C)/W_0(C) = -1$ should be obtained for even the smallest loops and not just as an asymptotic limit. On the other hand, if center vortices are rather thick in lattice units, and the location of P-plaquettes and center vortices is only weakly correlated, one would not expect such a striking difference in our values labeled "outside" and "outer ring," corresponding to a P-plaquette just outside or just inside the loop perimeter.

So it appears that the location of a P-plaquette is not a very good guide to the precise position of a thick center vortex. On the other hand, the presence of a single P-plaquette anywhere inside the loop tells us that the sign of a large SU(2) Wilson loop is, on average, negative. It seems that a P-plaquette inside a loop is strongly indicative of center flux passing through the loop, but does not give us much information about how that flux is distributed inside the minimal area.

ACKNOWLEDGMENTS

This work is supported in part by the U.S. Department of Energy under Grant No. DE-FG03-92ER40711.

[1] G. 't Hooft, **Nucl. Phys. B138, 1 (1978)**.
[2] G. Mack and V. Petkova, **Ann. Phys. (N.Y.) 125, 117 (1980)**.
[3] J. M. Cornwall, **Nucl. Phys. B157, 392 (1979)**.
[4] R. P. Feynman, **Nucl. Phys. B188, 479 (1981)**.
[5] H. B. Nielsen and P. Olesen, **Nucl. Phys. B160, 380 (1979)**.
[6] J. Ambjorn and P. Olesen, **Nucl. Phys. B170, 265 (1980)**.
[7] J. Greensite, *An Introduction to the Confinement Problem*, Lect. Notes Phys (Springer, New York, 2011), p. 821.
[8] J. Greensite, **Prog. Part. Nucl. Phys. 51, 1 (2003)**.
[9] E.-A. O'Malley, W. Kamleh, D. Leinweber, and P. Moran, **arXiv:1112.2490**.
[10] L. Del Debbio, M. Faber, J. Giedt, J. Greensite, and S. Olejnik, **Phys. Rev. D 58, 094501 (1998)**.
[11] K. Langfeld, **Phys. Rev. D 69, 014503 (2004)**.